Schisantherin A induces ferroptosis in non-small cell lung cancer through activation of the YAP/ACSL4/TfR signaling pathway

WENXIANG ZHU[1*], YEYANG CHEN[2*], XIANGJIAN WU[1*], XIAOYAN FU[1], YONGSHI HE[1], YUXIA MO[1], QINGHUA ZHU[1], MINGWEN TANG[1] and ZHIGUANG ZHAI[3]

[1]The Fourth Clinical Medical College, Department of Respiratory and Critical Care Medicine, Shenzhen Hospital of Traditional Chinese Medicine, Guangzhou University of Chinese Medicine, Shenzhen, Guangdong 518033, P.R. China; [2]School of Chinese Medicine, Studies and Applications of Internal Chinese Medicines, Hong Kong Baptist University, Hong Kong, SAR, P.R. China; [3]Institute of Basic Theory for Chinese Medicine, Basic Research Center for Prevention and Treatment of Viral Diseases with Traditional Chinese Medicine, China Academy of Chinese Medical Sciences, Beijing 100700, P.R. China

Received April 9, 2025; Accepted September 25, 2025

DOI: 10.3892/mmr.2025.13734

Abstract. Schisantherin A (Sch A), a compound derived from *Schisandra chinensis*, has anti-inflammatory, anti-tumor, neuroprotective and antifibrotic properties. However, to the best of our knowledge, the role of Sch A in non-small cell lung cancer (NSCLC) has not yet been reported. The purpose of the present study was to determine whether Sch A can prevent the development of NSCLC and to elucidate the underlying mechanisms involved. The results of the present study demonstrated that Sch A inhibited the viability of A549 and HCC827 cells. Furthermore, Sch A increased the intracellular Fe^{2+} level, reduced the mitochondrial membrane potential and depleted the glutathione content in lung cancer cells. These effects were reversed by the ferroptosis inhibitors ferrostatin-1 and deferoxamine. Bioinformatics analysis and reverse transcription-quantitative PCR results suggested that Sch A increased the mRNA levels of the transcription factor yes-associated protein (YAP). Additionally, Sch A upregulated the expression of YAP and ferroptosis-related proteins, including acyl-CoA synthase long-chain family member 4 (ACSL4) and transferrin receptor (TfR), in lung cancer cells. Silencing of YAP led to the downregulation of its downstream targets, ACSL4 and TfR, even in the presence of Sch A. *In vivo*, Sch A significantly inhibited subcutaneous tumor growth in nude mice. In conclusion, Sch A may activate the YAP/ACSL4/TfR signaling axis to induce ferroptosis in NSCLC cells, positioning it as a potential small-molecule therapeutic agent for NSCLC.

Correspondence to: Professor Zhiguang Zhai, Institute of Basic Theory for Chinese Medicine, China Academy of Chinese Medical Sciences, 16 Nanxiao Street, Dongcheng, Beijing 100700, P.R. China
E-mail: zhaizhiguang@mail.cintcm.ac.cn

*Contributed equally

Key words: schisantherin A, non-small cell lung cancer, ferroptosis, yes-associated protein/acyl-CoA synthase long-chain family member 4/transferrin receptor

Introduction

Primary lung cancer is the most common malignancy in China, with non-small cell lung cancer (NSCLC) being the most prevalent histological type, accounting for 80-85% of all cases (1). The all-stage combined 5-year relative survival for lung cancer in China is ~15% (2). The clinical treatment of NSCLC primarily involves a combination of chemotherapy (platinum-based doublets such as cisplatin-pemetrexed for non-squamous histology, cisplatin-gemcitabine or carboplatin-paclitaxel for squamous disease) and radiotherapy. In recent years, notable advances have been made in the diagnosis and treatment of NSCLC, driven by research into the molecular mechanisms (3,4). Targeted therapy has led to more successful outcomes in the treatment of NSCLC; however, despite the success of targeted therapies in disease control, for example, EGFR-mutant disease is treated with osimertinib, ALK-rearranged disease with alectinib/lorlatinib, ROS1-positive disease with entrectinib, and RET fusions with selpercatinib, the majority of patients with NSCLC develop resistance and experience disease progression, highlighting the persistent challenges in the treatment of NSCLC (5,6). To more effectively address these issues, ongoing efforts to screen for anticancer drugs and investigate novel therapeutic approaches are important in identifying more effective treatment strategies.

Ferroptosis is a recently discovered form of iron-dependent non-apoptotic cell death characterized by the accumulation of iron-dependent lipid peroxides and the loss of glutathione (GSH) peroxidase 4 activity (7). The Hippo/yes-associated protein (YAP)/transcriptional coactivator with PDZ-binding motif (TAZ) signaling pathway is a highly conserved protein kinase signaling pathway that regulates the phosphorylation status and nuclear localization of the downstream transcriptional coactivators YAP and TAZ (8,9). The Hippo/YAP/TAZ

pathway controls various cellular processes, including proliferation, apoptosis and organ morphology. As a key regulator linking ferroptosis and the tumor microenvironment (TME), the Hippo/YAP/TAZ signaling pathway influences the biological behavior and susceptibility of tumor cells to ferroptosis under the regulation of various non-genetic factors (8,9). Reports have suggested that the human gut absorbs 1-2 mg iron daily from dietary sources. Iron within cells is either stored in ferritin or exported into the plasma by iron transporters. In the presence of hepcidin, divalent iron is oxidized to ferric iron and binds to transferrin (Tf), which then associates with Tf receptors (TfRs) on the surface of target cell membranes, facilitating intracellular iron release and initiating iron cycling (9-11). When the iron concentration in tissues increases excessively and exceeds the binding capacity of Tf, non-Tf-bound iron (NTBI) is formed (9-11). NTBI, along with some unstable ferrous ions, can easily promote lipid peroxidation and H_2O_2 cleavage through Fenton and Haber-Weiss reactions, accelerating the formation of reactive oxygen species (ROS) and inducing ferroptosis. Furthermore, acyl-CoA synthase long-chain family member 4 (ACSL4) connects free polyunsaturated fatty acids (PUFAs) with acyl-CoA to form PUFA-CoA, which is then incorporated into phospholipids (PLs) by lysophosphatidylcholine acyltransferase 3 to generate PUFA-PL (10,11). The H_2O_2 and free iron in the cytoplasm undergo a Fenton reaction, producing ROS, which, in turn, oxidizes PUFA-PL on the cell membrane, leading to membrane rupture and ferroptosis (12,13). Studies have confirmed that ACSL4 is an important regulatory site in the Hippo/YAP/TAZ signaling pathway that mediates ferroptosis (12,13). Hence, the Hippo/YAP/TAZ signaling pathway serves an important role in regulating ferroptosis, and targeting this pathway may be an important therapeutic strategy for treating NSCLC.

Schisantherin A (Sch A) is a bioactive lignan isolated from the traditional Chinese medicine (TCM) *Schisandra chinensis* that has demonstrated notable pharmacological effects, such as anti-inflammatory, antitumor, neuroprotective and liver fibrosis-improving effects (14,15). Despite its known bioactivity, to the best of our knowledge, the specific role of Sch A in NSCLC has not yet been reported, making it an unexplored area with potential for revealing new therapeutic strategies. Given its diverse pharmacological effects, investigating Sch A in the context of NSCLC may provide valuable insights and offer a new option for targeted therapy in lung cancer, which remains a major clinical challenge.

Materials and methods

Cell culture. Procell Life Science & Technology Co., Ltd. provided the EGFR-mutant HCC827 cell line (human lung adenocarcinoma origin, harboring the classic EGFR Exon19del E746-A750 deletion mutation; cat. no. CL-0094) and the EGFR wild-type A549 cell line (cat. no. CL-0016). These cell lines were grown in an incubator at 37˚C with 5% CO_2. HCC827 cells were cultured in RPMI 1640 medium (HyClone; Cytiva) supplemented with 1% penicillin-streptomycin (Beijing Solarbio Science & Technology Co., Ltd.) and 10% fetal bovine serum (HyClone; Cytiva). A549 cells were grown in Ham's F-12K medium (Procell) supplemented with 1% penicillin-streptomycin and 10% fetal bovine serum.

Cell Counting Kit-8 (CCK-8) assay. A total of 3,000 A549 and HCC827 cells/well were plated into 96-well plates. After overnight incubation, various concentrations of Sch A (0.5, 1, 2, 4, 8, 16, 32, 64, 128 and 256 μg/ml; MilliporeSigma) were added to each well, with three replicates for each concentration. Drug-free medium served as a blank control for 48 h at 37˚C. Subsequently, 10 μl CCK-8 reagent (Beijing Solarbio Science & Technology Co., Ltd.) was added for 2-h incubation. Next, the absorbance was measured at 450 nm and the IC_{50} values were calculated using GraphPad Prism 10.0 (Dotmatics).

Inhibitor treatments. The following inhibitors were co-incubated with Sch A: Z-VAD-FMK (pan-caspase inhibitor; HY-16658B; final concentration: 20 μM); 3-Methyladenine (3-MA) (autophagy inhibitor, HY-19312; final concentration: 5 mM); Necrostatin-1 (Nec-1) (necroptosis inhibitor; MCE; HY-15760, 10 μM); Ferrostatin-1 (Fer-1) (ferroptosis inhibitor; MCE; HY-100579, 1 μM); Deferoxamine (DFO) (iron chelator/ferroptosis inhibitor; HY-B1625; all MCE; final concentration: 100 μM). Vehicle controls received matching volumes of DMSO (≤0.1% v/v). Cells (A549 and HCC827) were pretreated with inhibitors at 37˚C for 2 h, and then co-incubated with 6 μg/ml Sch A in A549 cells and 16 μg/ml Sch A in HCC827 cells together with the same inhibitors for an additional 24 h at 37˚C.

Detection of cell death by flow cytometry. In 6-well plates, A549 and HCC827 cells were plated at a density of $5x10^5$ cells/well and were incubated overnight. The cells were divided into Sch A-treated and control groups, with A549 cells treated with 6 μg/ml Sch A and HCC827 cells treated with 16 μg/ml Sch A for 48 h at 37˚C. The cells were collected using EDTA-free trypsin and then washed with 100 μl 1X binding buffer (Annexin V-PE/7-AAD Apoptosis Kit; E-CK-A216, Wuhan Elabscience Biotechnology Co., Ltd). A total of 5 μl each of Annexin V-APC and 7-AAD were used to stain the cells. Following 15 min of staining at room temperature in the dark, the cells in quadrant 3 were analyzed using a CytoFLEX S flow cytometer (Beckman Coulter, Inc.) and FlowJo v10 software (BD Biosciences).

Gene-set retrieval and intersection analysis. Ferroptosis- and NSCLC-associated genes were retrieved from GeneCards (genecards.org;). Venn diagram were generated using Venny 2.1 (https://bioinfogp.cnb.csic.es/tools/venny/), yielding the overlapping gene set for downstream analyses.

PPI network construction and key node identification. The overlapping genes were imported into the STRING database (v11.x; string-db.org) to build the PPI) network. Network topology (node degree) was used to prioritize key regulators; YAP1 emerged as a highly connected transcription factor within the network.

Cell cycle detection by flow cytometry. In 6-well plates, A549 and HCC827 cells were plated at a density of $5x10^5$ cells/well and incubated overnight at 37˚C. The cells were divided into Sch A-treated and control groups, with A549 cells treated with 6 μg/ml Sch A and HCC827 cells treated with 16 μg/ml Sch A for 48 h at 37˚C. For 12 h, A549 and HCC827 cells

were harvested and washed once with PBS, adjusted to $1x10^6$ cells/ml, and fixed with ice-cold 70% ethanol at 4˚C for 12 h. Fixed cells were washed with PBS, then incubated with 100 μl RNase A solution (DNA Content Quantitation Assay; Beijing Solarbio Science & Technology Co., Ltd.) at 37˚C for 30 min. A total of 400 μl PI staining solution was added and samples were incubated for 30 min at 4˚C before acquisition (Ex 488 nm). Next, flow cytometry (CytoFLEX S) was used to assess cell cycle progression, and FlowJo software was used to analyze the data.

Western blot analysis. A549 and HCC827 cells were seeded in 6-well plates at a density of $1x10^6$ cells/well, and the cells were grown for 24 h. After A549 and HCC827 cells were treated with 5, 10, 20, 40 μg/ml Sch A for 48 h at 37˚C, they were lysed in RIPA lysis buffer (Beijing Solarbio Science & Technology Co., Ltd.), and the supernatant was centrifuged at 11,000 g for 15 min at 4˚C to extract all the cellular protein. With a BCA kit, protein quantification was carried out (Beijing Solarbio Science & Technology Co., Ltd.). After being separated by SDS-PAGE on 12% gels, 20 μg proteins were transferred to a PVDF membrane (Thermo Fisher Scientific, Inc.). After three washes with 0.1% PBS-Tween (PBST), the membranes were blocked with 8% skimmed milk for 2 h at room temperature, after which the primary antibodies were added at 4˚C overnight. The primary antibodies used were against YAP (cat. no. 14074; 1:1,000; Cell Signaling Technology, Inc.), ACSL4 (cat. no. T510198, 1:1,000; Abmart Pharmaceutical Technology Co., Ltd.), TfR (T56618; 1:1,000; Abmart Pharmaceutical Technology Co., Ltd.) and GAPDH (2118, 1:5,000; Cell Signaling Technology, Inc.). The membranes were then incubated with an ActivAb Goat Anti-Rabbit IgG/HRP (1:4,000 dilution, Beijing Solarbio Science & Technology Co., Ltd.) at room temperature for 2 h following three PBST washes (5 min each). The blots were subsequently visualized with ECL western blotting substrate (Beijing Solarbio Science & Technology Co., Ltd.) for detection. GAPDH served as the internal reference and ImageJ2 (National Institutes of Health) was used to evaluate the density of the protein bands.

Detection of intracellular malondialdehyde (MDA), Fe^{2+} and GSH levels. After A549 and HCC827 cells were centrifuged at 10,000 x g for 10 min at 4˚C, the supernatant was collected. According to the manufacturer's instructions, the total intracellular levels of MDA, Fe^{2+} and GSH in 50 μl supernatant were determined via the MDA Content Assay Kit (cat. no. BC0025), Ferrous Ion Content Assay Kit (cat. no. BC5415) and Reduced GSH Content Assay Kit (BC1175; all Beijing Solarbio Science & Technology Co., Ltd.), respectively. The source of all the assay kits was Beijing Solarbio Science & Technology Co., Ltd.

Transfection of small interfering RNA (siRNA). Shanghai GenePharma Co., Ltd. constructed both negative control (NC) siRNA (forward: 5'-UUCUCCGAACGUGUCACGUTT-3'; reverse: 5'-ACGUGACACGUUCGGAGAATT-3') and YAP-targeting siRNA (si-YAP; forward: 5'-AUGUGAUUUAAGAAGUAUCUC-3'; reverse: 5'-GAGAUACUUCUUAAAUCACAU-3'). In 6-well plates, A549 and HCC827 cells were plated at a density of $1x10^5$ cells/well and cultured overnight. Transfections were performed with the siRNA-mate plus transfection kit (GenePharma; cat. no. G04026) following the manufacturer's instructions. Briefly, 15 pmol siRNA was mixed with Buffer (8.5 μl) to prepare the siRNA premix (final ~1.5 μM), combined with 3 μl siRNA-mate plus to form complexes, and added directly to each 24-well (30 nM siRNA in 0.5 ml complete medium). Cells were incubated with the transfection complexes at 37˚C in a humidified incubator with 5% CO_2 for 48 h without changing the medium. Subsequent experiments were performed immediately.

Reverse transcription-quantitative PCR (RT-qPCR). Using the Total RNA Extraction Kit (Beijing Solarbio Science & Technology Co., Ltd.), total RNA was extracted from each set of cells. A NanoDrop 2000 spectrophotometer (NanoDrop; Thermo Fisher Scientific, Inc.) was used to measure the concentration and purity of the RNA. For each sample, RT 1 μg total RNA into cDNA was performed with the HiScript II One Step RT-PCR Kit (Vazyme Biotech Co., Ltd.). The mRNA expression levels of prostaglandin-endoperoxide synthase 2 (ptgs2) and GSH-specific γ-glutamylcyclotransferase 1 (Chac1) were measured via AceQ qPCR SYBR Green Master Mix (without ROX) (Vazyme Biotech Co., Ltd.), with GAPDH serving as the internal reference gene. Thermocycling conditions were as follows: initial denaturation at 95˚C for 5 min; followed by 40 cycles of denaturation at 95˚C for 10 sec and annealing/extension at 60˚C for 30 sec. The $2^{-\Delta\Delta Cq}$ method was used to determine the relative expression levels of target genes (16). The primers are listed in Table I.

FerroOrange staining. After A549 and HCC827 cells were washed with serum-free medium, 500 μl 1 μM FerroOrange working solution (MedChemExpress) was added. The cells were then incubated at 37˚C in a 5% CO_2 incubator for 30 min. A fluorescence microscope (Olympus Corporation) was used to measure the fluorescence intensity.

JC-1 staining. After A549 and HCC827 cells were treated with 6 μg/ml Sch A and HCC827 cells treated with 16 μg/ml Sch A for 48 h at 37˚C, 100 μl JC-1 fluorescence staining solution [mitochondrial membrane potential (MMP) assay kit with JC-1; Beijing Solarbio Science & Technology Co., Ltd.] was added to each well at 37˚C for 20 min, and the A549 and HCC827 cells were incubated in the dark for 20 min. Subsequently, the cells were inspected under a fluorescence microscope (Olympus Corporation). Green fluorescence (excitation, 485 nm; emission, 535 nm; mono JC-1) was used to identify apoptotic or necrotic cells, whereas red fluorescence (excitation, 550 nm; emission, 600 nm; poly JC-1) was used to identify healthy cells.

Xenograft nude mouse tumor model. Following centrifugation and trypsin digestion, $5x10^{10}$/l serum-free DMEM (HyClone; Cytiva) was used to resuspend A549 cells at 300 x g for 5 min at 4˚C. All BALB/c nude mice were maintained at 22±2˚C, 50±10% relative humidity, under a 12:12-h light/dark cycle, with free access to autoclaved chow and water. Mice were acclimated for at least 7 days prior to inoculation. The right axilla of male BALB/c nude mice (n=10; age, 6-weeks; weight, 16-18 g; Beijing Vital River Laboratory Animal Technology

Table I. Primer sequences.

Primer	Sequence (5'-3')
GAPDH-F	GGGGAGCCAAAAGGGTCATC
GAPDH-R	TGGTTCACACCCATGACGAA
YAP1-F	ACATTGCAAAAGTGGGTGGC
YAP1-R	TGCGAGGATAAAATCCACCTGA
FOXO1-F	AACCCCAGCCCCAACTTAAA
FOXO1-R	ACCTCAAGGAGAGGCCAACT
FOXP1-F	GGCTTCCCTCTGTGTGTTG
FOXP1-R	ATGGGGAAGGGTTAGGCTGA
FOXA2-F	CAAACAGAGGGCCACACAGA
FOXA2-R	CGAGACCTGGATTTCACCGT
FOXN4-F	GTTCCGCAGATAGCTGGGTT
FOXN4-R	AGCTTTGCTGGGAGAGCATT
HIF1A-F	GTCACTTTGCCAGCTCAAAAGA
HIF1A-R	ACCAACAGGGTAGGCAGAAC
RELA-F	GGCATTGTCCCTGTGCCTAA
RELA-R	GAAGTCCCAGACCAAACCCC
STAT3-F	CAAAACCACCTTGCCTCAGC
STAT3-R	GGCTCAGCTCCTCTCAGAAC
CEBPA-F	GGACCCTCAGCCTTGTTTGT
CEBPA-R	AGACGCGCACATTCACATTG
MYC-F	TGGCTGCTTGTGAGTACAGG
MYC-R	TGAACTGGCTTCTTCCCAGG
SP1-F	ATTGTGGACAAGGGCAGGTC
SP1-R	CAACAGTGGTGTGGACTGGT
JUN-F	TCCTGCCCAGTGTTGTTTGT
JUN-R	GACTTCTCAGTGGGCTGTCC
TP53-F	GGAAATCTCACCCCATCCCA
TP53-R	GCAGATGTGCTTGCAGAATGT
NFE2L2-F	TCCCTGCAGCAAACAAGAGA
NFE2L2-R	AACTAGCCCAAATGGTGTCCT
AP-1-F	TCCTGCCCAGTGTTGTTTGT
AP-1-R	GACTTCTCAGTGGGCTGTCC
PPARA-F	TGACAGAAACACACGCGAGA
PPARA-R	CGCTCTTCTCTGCACATCCT
NRF1-F	TCTCCACGTCTTGCTCAACC
NRF1-R	ATCCATGCTCTGCTACTGGG
GATA3	TTGCCGTTGAGGGTTTCAGA
GATA3	GCACGCTGGTAGCTCATACA
KLF2-F	GTCTGGAAACCCACCTGGAG
KLF2-R	TTGGTGGTCATGGTTACCCG
RUNX3-F	CTGTAAGGCCCAAAGTGGGT
RUNX3-R	CAGTTTCCACCCAGCTCCAT
BACH1-F	ACAGGTTGCATGTGGACACT
BACH1-R	TCACCTGAGAATTCACCGTAACA
ZEB1-F	CAACAAGCCTGAACTGCTGTC
ZEB1-R	GCAGGATGACAATGTACCCCA

AP-1, activator protein 1; BACH1, BTB domain and CNC homolog 1; CEBPA, CCAAT/enhancer binding protein alpha; GATA3, GATA binding protein 3; HIF1A, Hypoxia-inducible factor 1 subunit alpha; KLF2, Kruppel like factor 2; NFE2L2, NF-E2 like bZIP transcription factor 2; NRF1, Nuclear respiratory factor 1; PPARA, Peroxisome proliferator activated receptor alpha; RELA, RELA proto-oncogene, NF-KB subunit; RUNX3, RUNX family transcription factor 3; SP1, Sp1 transcription factor; YAP1, Yes-associated protein 1; ZEB1, Zinc finger E-box binding homeobox 1.

Co., Ltd.; Charles River Laboratories, Inc.) was then aseptically injected with a 0.1-ml aliquot of the cell mixture (each mouse received an injection of $5x10^6$ A549 cells). According to relevant studies on lung cancer models (17,18), sex has a minimal impact on experimental results; therefore, sex was not considered a variable in the present study. After ~14 days, the tumor model was considered successfully established once the maximum tumor diameter was >5 mm or the tumor volume was >50 mm^3.

Humane endpoints included maximum tumor diameter ≥15 mm, tumor volume ≥1,500 mm^3, ulceration/necrosis/infection, ≥20% body weight loss, or failure to eat/drink. No mice reached humane endpoints before planned termination. The mice with successfully established tumors were randomly assigned to two groups: A control group and a Sch A treatment group. During the 14-day treatment period, the Sch A group of mice were given Sch A orally at a dose of 10 mg/kg/day, whereas the control group was given an equivalent volume of saline. Following treatment, the long and short diameters of the xenograft tumors were measured, and their volumes were computed using the following formula: Tumor volume=(long diameter x short $diameter^2$)/2. In the present study, the maximum tumor diameter observed was 8.2 mm, and the maximum tumor volume was 107 mm^3. Isoflurane anesthesia was administered at a concentration of 4% for induction and 1.5% for maintenance, with an oxygen flow rate of 1.5 l/min, during subcutaneous tumor cell injection and tumor measurement procedures. For oral gavage, anesthesia was not employed, as this procedure is generally considered minimally invasive and does not typically require anesthesia. The mice were anesthetized with 4% isoflurane 1 h after the final administration and euthanized by decapitation. The tumors were then removed and weighed for analysis.

The present study was conducted in accordance with the Animal Research: Reporting of *In Vivo* Experiments guidelines and the Guide for the Care and Use of Laboratory Animals (US National Research Council) (19). All animal experiments were approved by the Committee on the Ethics of Animal Experiments of Guangzhou University of Chinese Medicine (Shenzhen, China; approval no. 2024055R).

Statistical analysis. SPSS 22.0 (IBM Corp.) was used to analyze the experimental data, and the results are presented as the mean ± SD of ≥3 independent experimental repeats. Pairwise comparisons were performed using the unpaired Student's t-test, and group comparisons were performed with one-way ANOVA followed by Tukey's post hoc analysis. $P<0.05$ was considered to indicate a statistically significant difference.

Results

Concentration- and time-dependent inhibition of A549 and HCC827 cell viability by Sch A. The viability of A549 and HCC827 cells was evaluated following exposure to a range of Sch A concentrations. The CCK-8 assay revealed a concentration-dependent decrease in viability in both cell lines (Fig. 1A and B). The IC_{50} values of Sch A were determined to be 6.53 μg/ml for A549 cells and 16.38 μg/ml for HCC827 cells. Based on these results, concentrations of 6 and 16 μg/ml were selected for subsequent experiments in A549

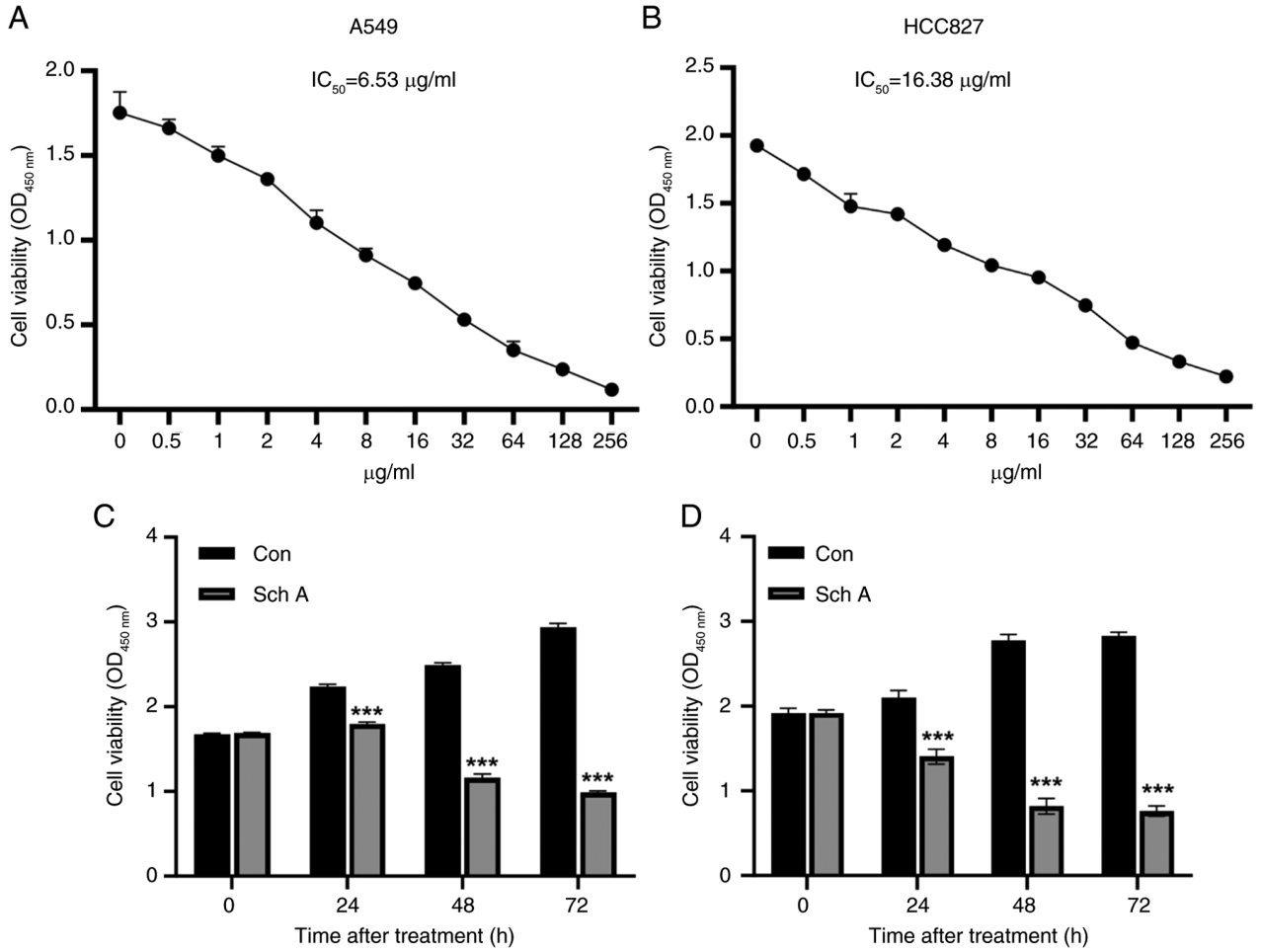

Figure 1. Lung cancer cell viability is suppressed by Sch A in a concentration- and time-dependent manner. Sch A decreased (A) A549 and (B) HCC827 cell viability in a concentration-dependent manner, according to Cell Counting Kit-8 analysis. Sch A significantly reduced the viability of (C) A549 and (D) HCC827 cells at 24, 48 and 72 h. ***P<0.001 vs. Con. Con, control; Sch A, Schisantherin A; OD, optical density.

and HCC827 cells, respectively. Furthermore, the inhibitory effect of Sch A on the viability of both cell lines increased significantly with prolonged treatment (Fig. 1C and D).

Fer-1 and deferoxamine (DFO) abolish Sch A-induced lung cancer cell death. Compared with the control, treatment with Sch A significantly increased late apoptosis in both A549 and HCC827 cells (Fig. 2A and B). Additionally, cell cycle analysis revealed a substantial accumulation of A549 and HCC827 cells in the G_1 phase, accompanied by a notable reduction in the percentage of cells in the S and G_2 phases (Fig. 2C and D). Upon preincubation for 1 h with a range of inhibitors, including the apoptosis inhibitor Z-VAD-FMK, the autophagy inhibitor 3-methyladenine, the necrosis inhibitor necrostatin-1 and the ferroptosis inhibitors Fer-1 and DFO, only the latter two inhibitors partially reversed the Sch A-induced reduction in cell viability. By contrast, apoptosis, autophagy and necrosis inhibitors had no significant effect on Sch A-induced cell death, highlighting the specific involvement of ferroptosis in this process (Fig. 2E and F).

Sch A induces ferroptosis in A549 and HCC827 cells by modulating MMP and lipid peroxidation. Changes were also observed in the MMP, where Sch A treatment led to a decrease in JC-1 aggregation and an increase in monomeric JC-1 levels, indicating a reduction in the MMP compared with that in the control group (Fig. 3A and B). Preincubation with the ferroptosis inhibitors Fer-1 and DFO resulted in a reduction in monomeric JC-1 levels and an increase in polymeric JC-1 levels, suggesting the restoration of the MMP. Furthermore, Sch A treatment led to elevated MDA levels in both A549 and HCC827 cells, an effect that was reversed by pre-treatment with Fer-1 and DFO (Fig. 3C and D). Sch A also caused a decrease in GSH levels in both cell lines, which was reversed by pre-treatment with Fer-1 and DFO (Fig. 3E and F). Additionally, an increase in the expression of the ferroptosis markers Chac1 and ptgs2 was observed following Sch A treatment, with Fer-1 and DFO effectively reversing the Sch A-induced upregulation of these markers (Fig. 3G and H).

Sch A upregulates YAP1 and modulates ferroptosis in NSCLC through transcriptional activation of ferroptosis-related proteins. Using GeneCards, an intersection analysis of ferroptosis-related and NSCLC-associated target genes revealed 739 overlapping genes, suggesting that these genes may serve an important role in regulating ferroptosis within NSCLC (Fig. 4A). Among these 739 overlapping genes, transcription factors were further analyzed to identify key node genes, with

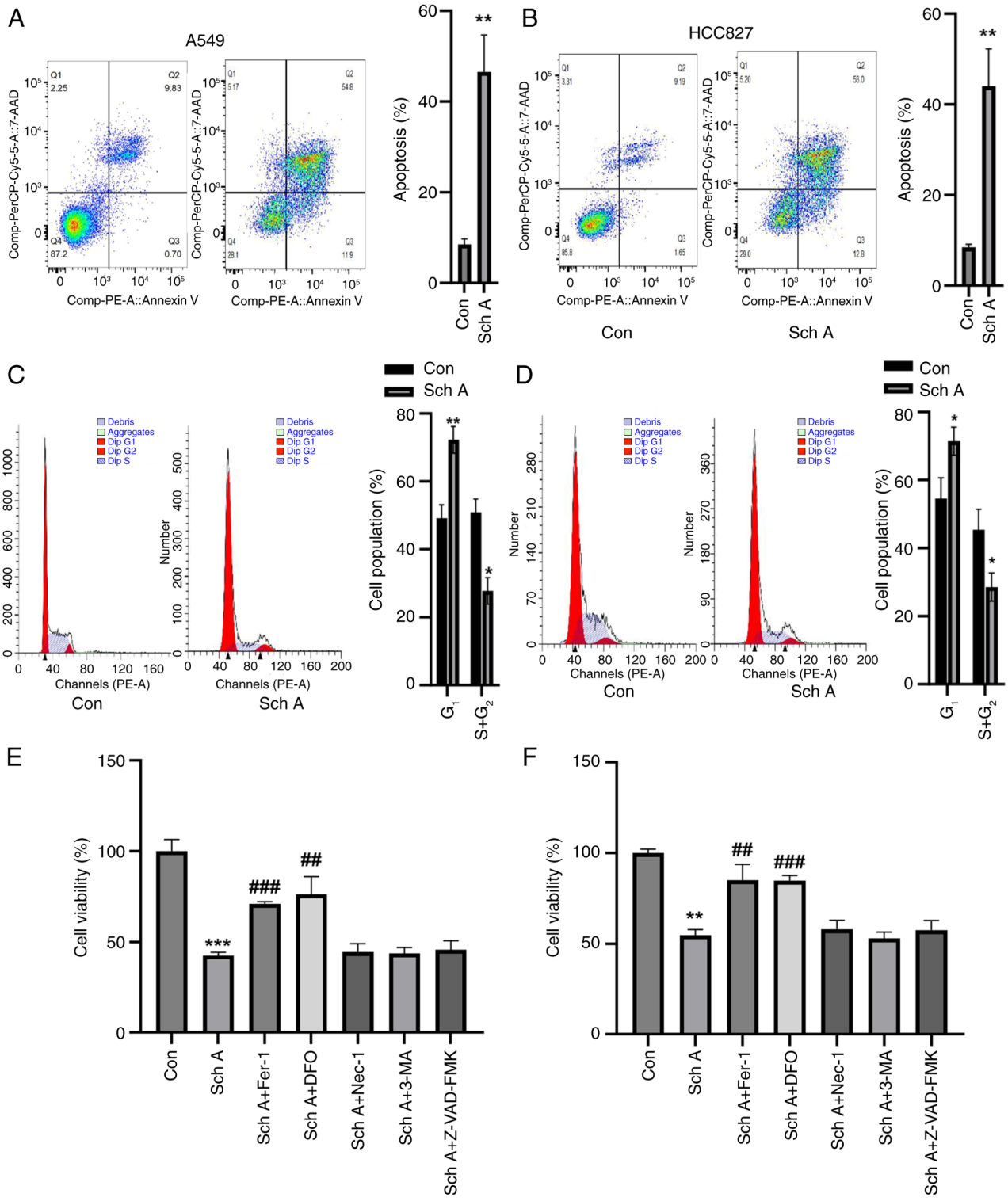

Figure 2. Sch A induces cell death and cell cycle arrest in A549 and HCC827 cells. Sch A considerably increased the death of (A) A549 and (B) HCC827 cells in comparison with the control group, according to flow cytometric analysis. Compared with Con, (C) A549 and (D) HCC827 cells presented a significant decrease in the number of G_2 + S-phase cells and a significant increase in the number of G_1-phase cells. Fer-1 and DFO were able to significantly reverse the Sch A-induced decrease in (E) A549 and (F) HCC827 cell viability, according to the results of the Cell Counting Kit-8 analysis. *P<0.05, **P<0.01 and ***P<0.001 vs. Con; $^{\#\#}$P<0.01 and $^{\#\#\#}$P<0.001 vs. Sch A. DFO, deferoxamine; Con, control; Sch A, Schisantherin A; Fer-1, ferrostatin-1; Nec-1, necrostatin-1; 3-MA, 3-methyladenine.

YAP emerging as a critical regulator within this intersecting gene network, highlighting its potential role in modulating ferroptosis in NSCLC (Fig. 4B). RT-qPCR analysis revealed that Sch A treatment of A549 and HCC827 cells led to a significant increase in YAP1 mRNA expression, indicating that Sch A can upregulate YAP1 in NSCLC cell lines (Fig. 4C and D). Given the multifaceted role of the Hippo pathway in regulating tumor cell behavior, the phosphorylation status of YAP, a key downstream effector of this pathway, was further examined. Although no changes in YAP phosphorylation levels were

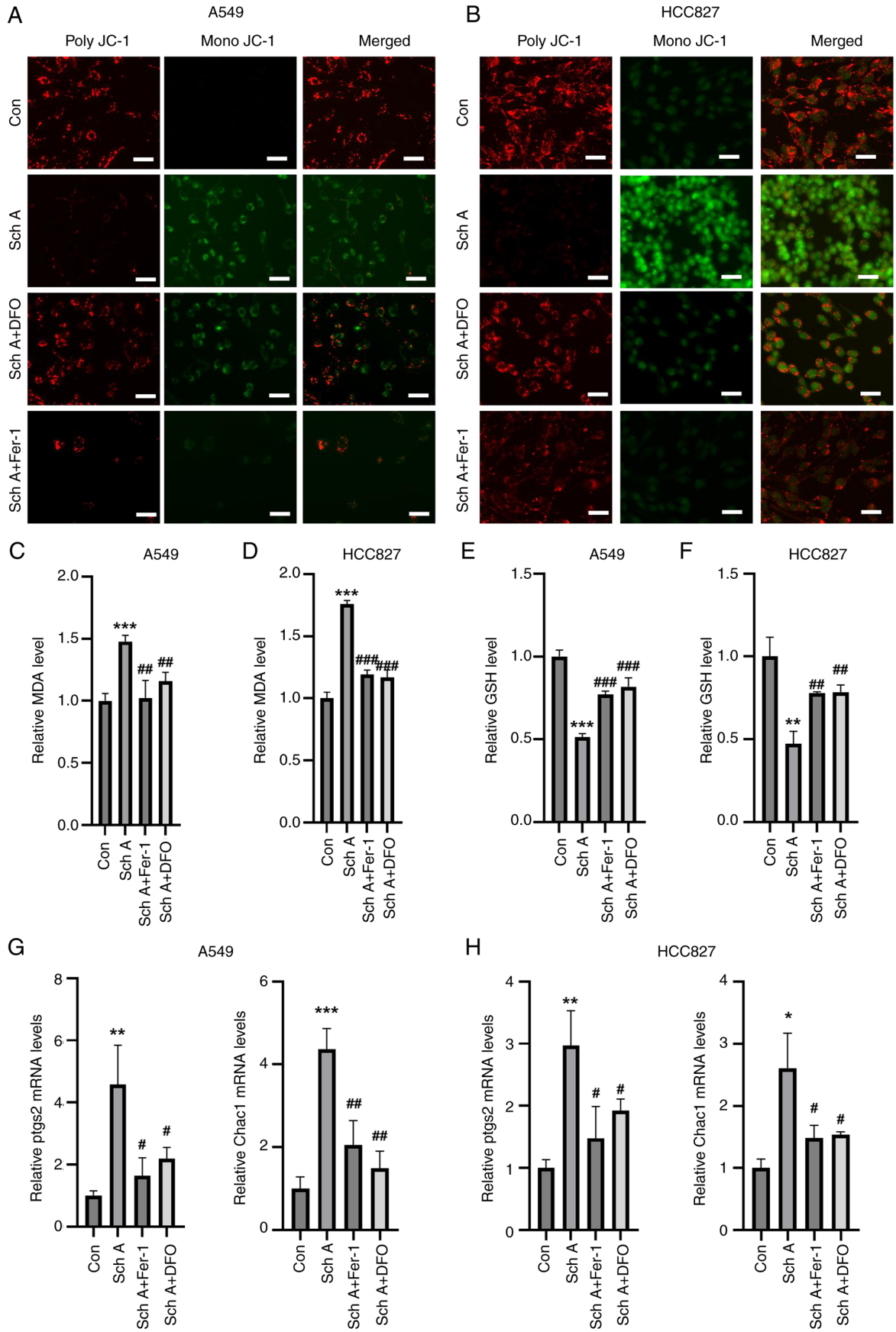

Figure 3. In A549 and HCC827 cells, ferroptosis inhibitors prevent Sch A-induced apoptosis. Fer-1 and DFO were shown by JC-1 staining to reverse the Sch A-induced MMP reduction in (A) A549 and (B) HCC827 cells (scale bar, 30 μm). Fer-1 and DFO inhibited the Sch A-induced increase in MDA in (C) A549 and (D) HCC827 cells. Fer-1 and DFO counteracted the Sch A-induced reduction in GSH in (E) A549 and (F) HCC827 cells. Reverse transcription-quantitative PCR analysis revealed that Fer-1 and DFO reversed the Sch A-induced increase in Chac1 and ptgs2 levels in (G) A549 and (H) HCC827 cells. *P<0.05, **P<0.01 and ***P<0.001 vs. Con; $^{\#}$P<0.05, $^{\#\#}$P<0.01 and $^{\#\#\#}$P<0.001 vs. Sch A. Con, control; Chac1, glutathione-specific γ-glutamylcyclotransferase 1; ptgs2, prostaglandin-endoperoxide synthase 2; Fer-1, ferrostatin-1; DFO, deferoxamine; Sch A, Schisantherin A; MDA, malondialdehyde; GSH, glutathione.

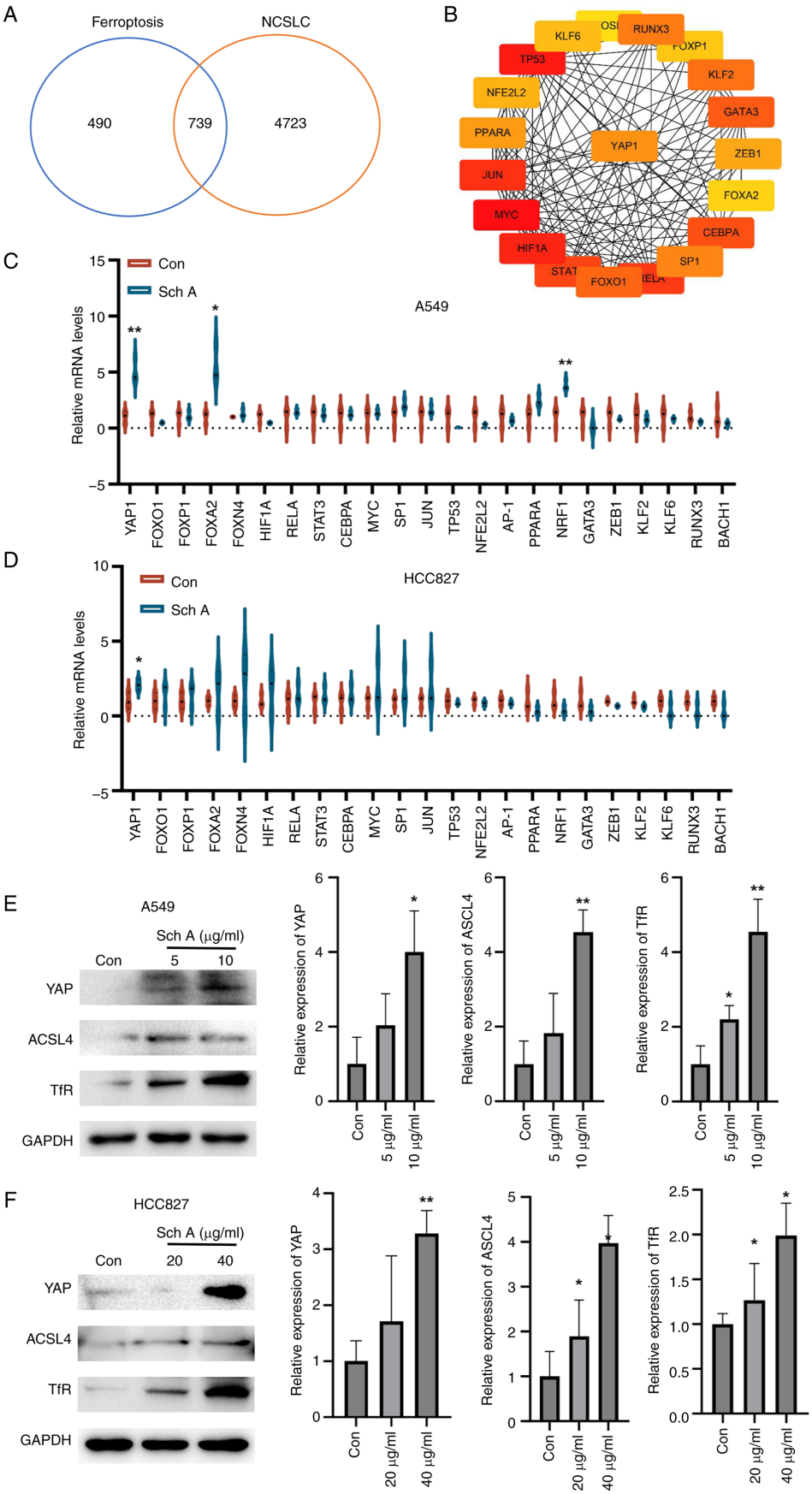

Figure 4. Sch A induces ferroptosis in lung cancer cells by activating YAP signaling. (A) GeneCards intersection analysis revealed 739 overlapping genes associated with both ferroptosis and NSCLC. (B) Transcription factors among the intersecting genes were analyzed to identify key node genes. Reverse-transcription-quantitative PCR analysis revealed that Sch A increased the mRNA expression levels of YAP1 in (C) A549 and (D) HCC827 cells. Western blot analysis revealed that Sch A increased the expression levels of TfR, ACSL4 and YAP in (E) A549 and (F) HCC827 cells. *P<0.05 and **P<0.01 vs. Con. Con, control; YAP, yes-associated protein; Sch A, Schisantherin A; TfR, transferrin receptor; ACSL4, acyl-CoA synthase long-chain family member 4; NSCLC, non-small cell lung cancer.

observed (data not shown), a marked increase in YAP protein levels was detected (Fig. 4E and F), suggesting that YAP may participate in ferroptosis through mechanisms independent of phosphorylation. To further investigate this finding, it was hypothesized that YAP might regulate ferroptosis by transcriptionally activating ferroptosis-related proteins, specifically TfR and ACSL4. Western blot analysis confirmed the involvement of YAP in regulating ferroptosis, as Sch A treatment increased the expression of the ferroptosis-related proteins TfR and ACSL4.

YAP knockdown abolishes Sch A-induced ferroptosis in lung cancer cells. To determine whether YAP activation has a role in Sch A-induced ferroptosis, the present study employed siRNAs targeting YAP. Western blot analysis demonstrated that transfection with si-YAP resulted in a marked reduction in the protein levels of YAP in both A549 and HCC827 cell lines when compared with cells transfected with the NC siRNA (Fig. 5A and B). The results, presented in Fig. 5A and B, demonstrated a significant reduction in YAP expression in both A549 and HCC827 cells following siRNA transfection, indicating efficient knockdown of YAP. Along with the knockdown of YAP, the downstream targets ACSL4 and TfR were also significantly suppressed by si-YAP. Following Sch A treatment conditions, si-YAP was still able to efficiently knock down YAP expression as well as the downstream targets ACSL4 and TfR in both cell lines. FerroOrange staining revealed that Sch A treatment led to notable Fe^{2+} accumulation in both A549 and HCC827 cells. However, upon YAP silencing, this increase in Fe^{2+} was effectively reversed, further indicating that YAP serves an important role in regulating iron metabolism during Sch A-induced ferroptosis (Fig. 5C and D). Additionally, quantification of Fe^{2+} and MDA levels in A549 and HCC827 cells revealed that Sch A treatment significantly elevated both Fe^{2+} and MDA levels compared with those in the control group, whereas YAP silencing effectively alleviated these Sch A-induced increases (Fig. 5E and F).

Sch A inhibits tumor growth in nude mice. To assess the effect of Sch A on tumor growth *in vivo*, a nude mouse xenograft model was used. Compared with the control treatment, Sch A treatment resulted in a significant reduction in both tumor mass and volume, demonstrating its potent inhibitory effect on tumor growth in this animal model (Fig. 6A and B). Furthermore, Sch A treatment led to a marked increase in MDA levels and Fe^{2+} accumulation within the tumors, indicating the promotion of ferroptosis-related oxidative stress and iron overload in the TME (Fig. 6C and D). This increase was accompanied by a significant decrease in GSH levels, suggesting a depletion of antioxidant defenses in the tumor tissues (Fig. 6E). Additionally, Sch A treatment upregulated the protein expression levels of YAP, ACSL4 and TfR in tumor tissues, which was consistent with the *in vitro* findings, further supporting the involvement of these proteins in Sch A-induced ferroptosis and tumor suppression (Fig. 6F).

Discussion

Lung cancer poses a notable threat to global human health and life, with >50% of patients being diagnosed at advanced stages, leading to a low chance of curative surgery (20). Currently, chemotherapy and radiotherapy are the primary treatment methods for lung cancer, but owing to their pronounced toxic side effects and the tendency for drug resistance to develop, patients often find it difficult to adhere to treatment, resulting in low cure rates and high recurrence rates (20,21). In recent years, TCM has attracted notable attention from researchers due to its potent therapeutic effects, low toxicity and multi-targeted approach for tumor treatment (14). Sch A, a major bioactive lignan isolated from the TCM plant *Schisandra chinensis*, has been shown to inhibit hepatocellular carcinoma cell proliferation by suppressing glucose metabolism, thereby exerting anti-liver cancer effects (22). Additionally, Sch A induces ROS generation, activates the JNK signaling pathway and inhibits nuclear factor erythroid 2-related factor 2, effectively suppressing gastric cancer cell proliferation and migration, and promoting apoptosis (23). However, to the best of our knowledge, no studies to date have reported the potential anticancer effects of Sch A on NSCLC and its underlying mechanisms.

To the best of our knowledge, the present study explored the molecular mechanisms underlying the anticancer effects of Sch A in NSCLC for the first time. The present results demonstrated that Sch A effectively inhibited the viability of NSCLC cells in a dose- and time-dependent manner. Treatment with Sch A significantly led to an increase in NSCLC cell apoptosis and induced cell cycle arrest, highlighting its notable anticancer activity. Further mechanistic investigations revealed that Sch A triggered ferroptosis in NSCLC cells, as supported by the reversal of the Sch A-induced reduction in cell viability and MMP loss upon treatment with the ferroptosis inhibitors Fer-1 and DFO. Additionally, Sch A treatment resulted in elevated intracellular levels of Fe^{2+} and MDA, alongside a significant decrease in the content of GSH, a key indicator of ferroptosis activation (24). Collectively, these findings provide evidence that Sch A induces ferroptosis in lung cancer cells, suggesting its potential as a novel therapeutic strategy for NSCLC.

Xian *et al* (25) and Zhu *et al* (26) reported that Sch A can induce apoptosis in NSCLC by inhibiting EGFR phosphorylation or synergizing with gefitinib. However, the present study was, to the best of our knowledge, the first to demonstrate that Sch A triggered ferroptosis through activation of the YAP/ACSL4/TfR axis, a cell death mechanism unexplored in prior research. While previous work, such as the study by Zhu *et al* (26), focused on apoptosis or, in the case of the study by Xian *et al* (25), apoptosis and cell cycle arrest, the systematic inhibitor screening experiments performed in the present study established ferroptosis as the predominant cell death modality under Sch A monotherapy, with the apoptosis inhibitor Z-VAD-FMK showing no significant effect on Sch A-induced cytotoxicity. To ensure translational relevance across NSCLC subtypes, two genetically distinct cell lines were employed, A549 (EGFR-wild type) and HCC827 (EGFR Exon19del E746-A750 mutant), which are tyrosine kinase inhibitor-sensitive lines frequently used in targeted-therapy studies (27,28). The results of the present study demonstrated that Sch A induced ferroptotic features in both cell lines, suggesting that its mechanism was not dependent on the EGFR mutation status and may therefore offer therapeutic potential

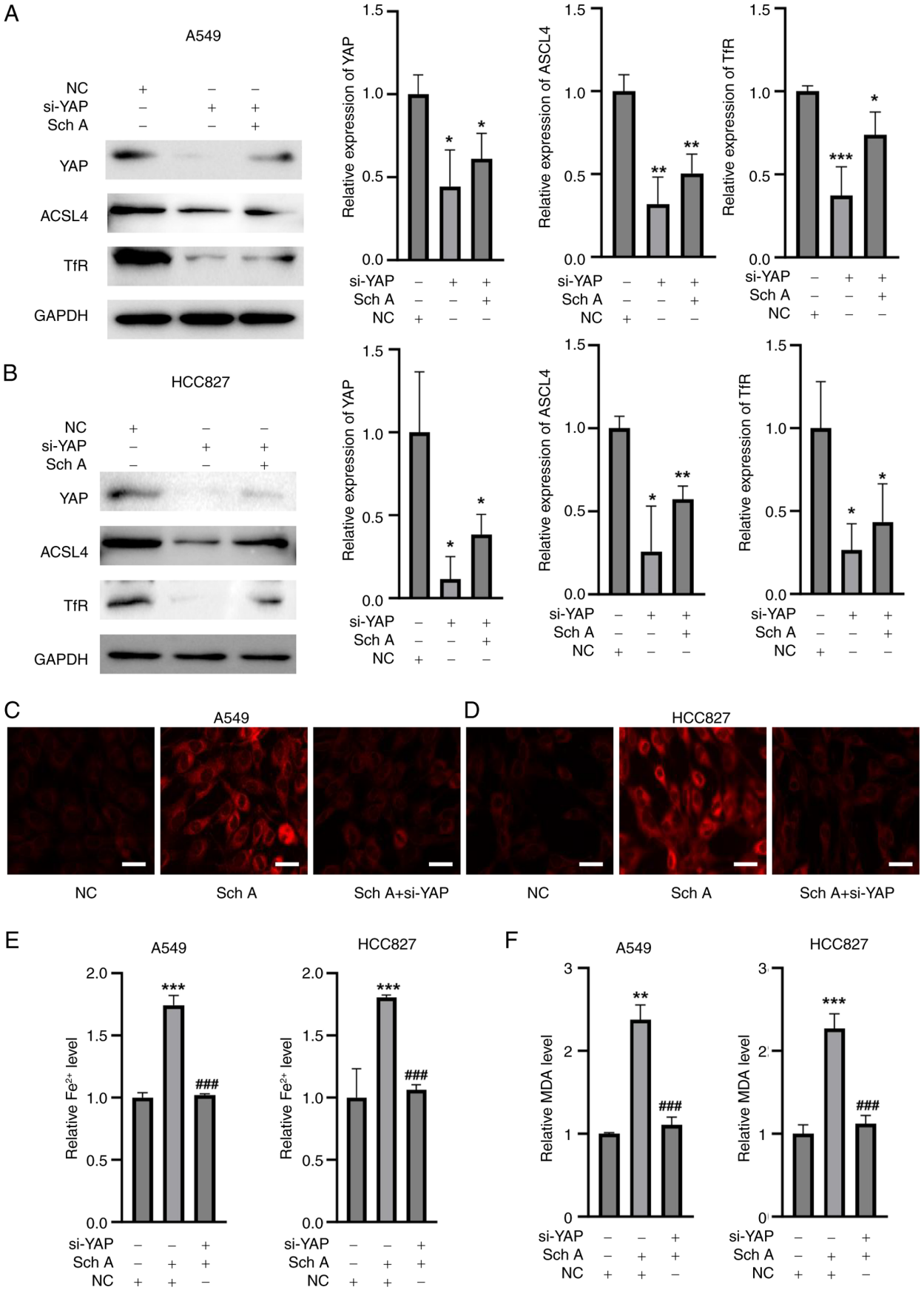

Figure 5. Silencing of YAP reverses Sch A-induced ferroptosis. Western blot analysis showed that the expression of YAP was decreased in (A) A549 and (B) HCC827 cells. In (C) A549 and (D) HCC827 cells, si-YAP decreased the expression of YAP and downstream signaling molecules. Fe^{2+} accumulation was induced by Sch A in (E) A549 and (F) HCC827 cells, and the increase in Fe^{2+} was reversed by YAP silencing, as demonstrated by FerroOrange staining (scale bar, 10 μm). After silencing YAP, the Sch A-induced increase in Fe^{2+} and MDA in (G) A549 and (H) HCC827 cells was reduced. *P<0.05, **P<0.01 and ***P<0.001 vs. NC; $^{\#\#\#}$P<0.001 vs. Sch A. NC, negative control; YAP, yes-associated protein; Sch A, Schisantherin A; si, small interfering RNA; MDA, malondialdehyde; ACSL4, acyl-CoA synthase long-chain family member 4; TfR, transferrin receptor.

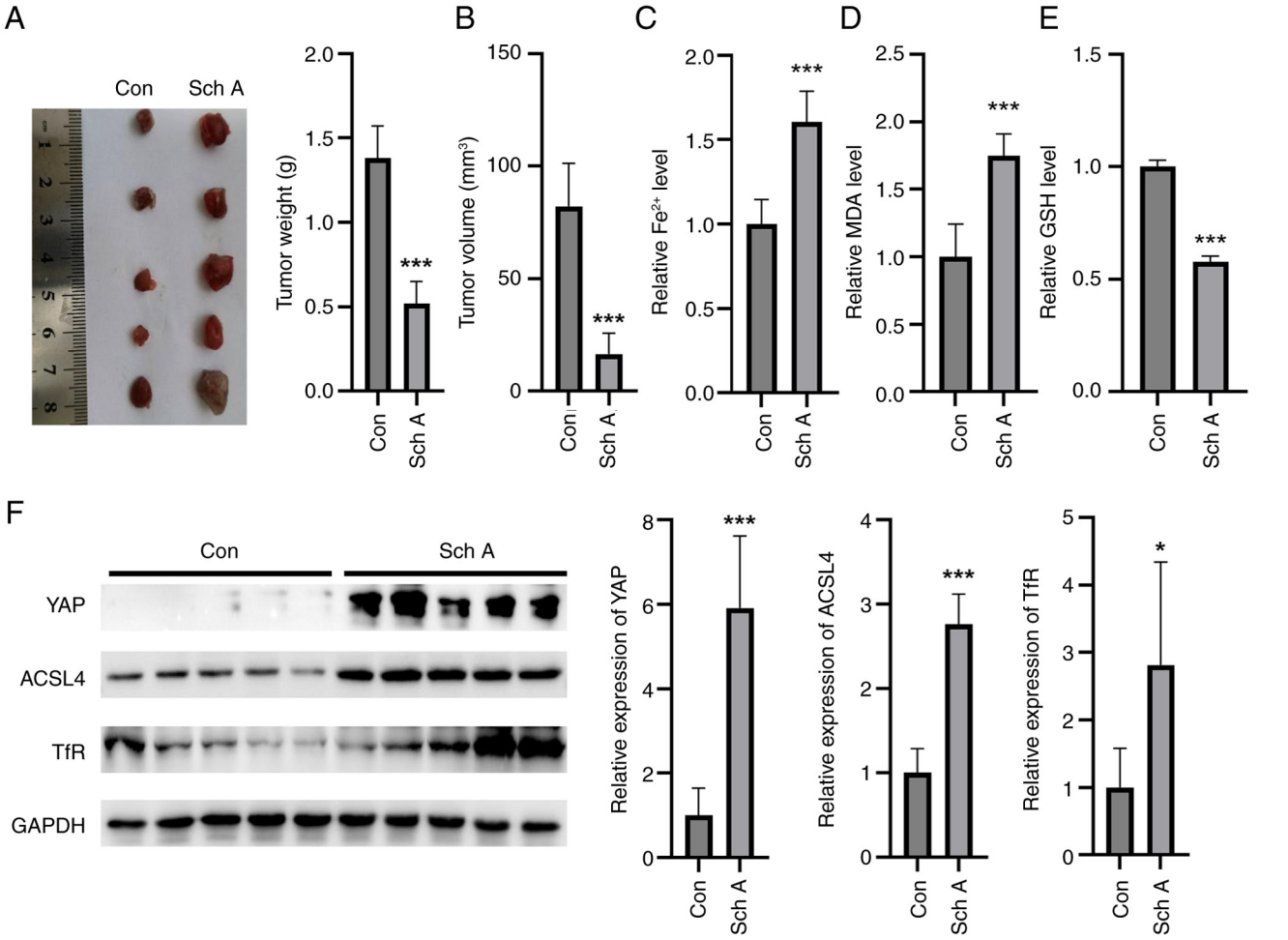

Figure 6. *In vivo*, Sch A prevents the formation of tumors in nude mice. Compared with Con, Sch A inhibited (A) tumor mass and (B) volume *in vivo* in nude mice. Sch A increased the (C) Fe^{2+} and (D) MDA contents in nude mouse tumors. (E) Sch A diminished the GSH levels in the tumors compared with those in the Con group. (F) Compared with those in the Con group, Sch A induced the expression levels of YAP, ACSL4 and TfR in the tumors of nude mice. *P<0.05 and ***P<0.001 vs. Con. Con, control; Sch A, Schisantherin A; MDA, malondialdehyde; GSH, glutathione; YAP, yes-associated protein; ACLS4, acyl-CoA synthase long-chain family member 4; TfR, transferrin receptor.

across a range of NSCLC genetic backgrounds. Notably, comparable increases in Fe^{2+} accumulation, and ACSL4 and TfR expression were observed in both A549 and HCC827 cells following Sch A treatment, indicating genotype-independent vulnerability to ferroptosis. The apparent discrepancy with the apoptotic phenotype described in the study by Zhu *et al* (26) may arise from key methodological differences: i) The aforementioned study used 50 μM Sch A for 24 h to induce apoptosis, whereas the present study employed lower concentrations that may activate distinct cell death pathways; and ii) the study by Zhu *et al* (26) quantified total apoptosis (quadrants 2 + 3) via a FITC-PE kit, whereas the present study specifically analyzed late apoptosis (quadrant 3) via an Annexin V-7-AAD kit alongside ferroptosis markers, such as Fe^{2+} accumulation. The Annexin V-FITC-PE approach cannot exclude interference from necrotic or ferroptotic cells in PI^{+} populations, which represent membrane-disrupted cells. By contrast, the Annexin V-7-AAD kit precisely distinguishes early apoptosis (quadrant 3, Annexin V^{+}/7-AAD^{-}), late apoptosis (quadrant 2, Annexin V^{+}/7-AAD^{+}) and primary necrosis (quadrant 1, Annexin V^{-}/7-AAD^{+}). The present study observed a significant Sch A-induced increase in 7-AAD^{+} cells in quadrant 2 (late apoptosis/secondary necrosis), which co-occurred with ferroptosis biomarkers. Combined with specific rescue by the ferroptosis inhibitors Fer-1 and DFO, the present study concluded that ferroptosis, not classical apoptosis, was the primary death mechanism. The present study explored the anticancer mechanism of Sch A in NSCLC, which shifted the paradigm from apoptosis to YAP-dependent ferroptosis. Hence, the present study investigated a novel signaling axis with broad therapeutic implications, advancing the potential of Sch A as a precision oncology agent.

Furthermore, emerging evidence links EGFR signaling to ferroptosis regulation (29,30). In colorectal cancer, glucose deprivation inhibits Hippo signaling and activates EGFR, which enhances cell anti-ferroptotic defenses through PPAR-ACSL1/4 lipid-metabolic remodeling, thereby limiting lipid peroxidation (29). In triple-negative breast cancer, EGFR inhibition promotes ferroptosis via YAP/mTOR-mediated autophagy (30). In the NSCLC models of the present study, Sch A-induced YAP activation led to the upregulation of ACSL4 and TfR, which are hallmark mediators of ferroptosis, in both EGFR-mutant (HCC827) and -wild-type (A549) cells, indicating YAP-driven ferroptosis across distinct

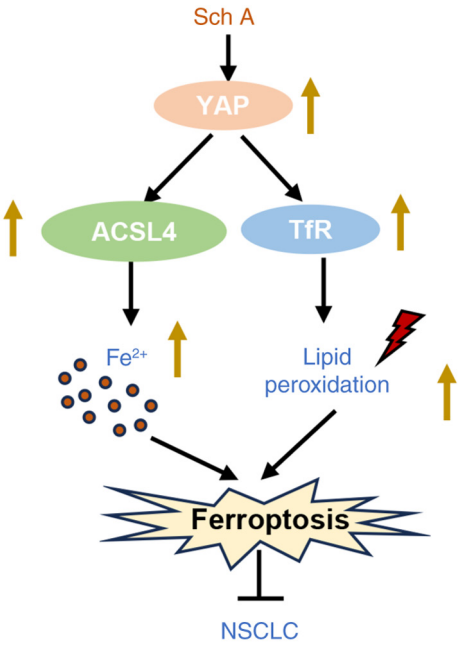

Figure 7. Schematic diagram showing the molecular mechanism by which Sch A suppresses NSCLC. Sch A, Schisantherin A; NSCLC, non-small cell lung cancer; YAP, yes-associated protein; ACSL4 acyl-CoA synthase long-chain family member 4; TfR, transferrin receptor.

EGFR backgrounds. This cascade may have been modulated by the tissue context and EGFR mutational status but ultimately converged on a shared ferroptotic axis. In summary, the present study provided new mechanistic insight into the anti-NSCLC potential of Sch A. By demonstrating consistent ferroptosis induction across both EGFR-wild-type and mutant backgrounds, the present study highlighted the promise of Sch A as a mutation-agnostic therapeutic.

While traditional molecular research has revealed that Sch A induced ferroptosis in NSCLC cells via the YAP/ACSL4/TfR axis, this perspective alone may not have fully accounted for complex clinical phenomena such as drug resistance and tumor recurrence. By adopting the cancer ecology paradigm (31), the role of Sch A within the TME was interpreted as part of a dynamic ecological system. In this context, YAP may function not only as a molecular signaling node but also as an ecological sensor that enables cancer cells to perceive and adapt to microenvironmental stresses. For example, under glucose-deprived conditions, which are common in advanced NSCLC, YAP activation typically confers survival advantages to cancer cells by promoting metabolic reprogramming (32). However, the present findings suggested that Sch A disrupted this adaptive mechanism by potentially activating YAP, leading to the upregulation of ACSL4 and TfR expression. This shift triggered mitochondrial lipid peroxidation and induced ferroptosis, effectively converting the adaptive evolution of cancer cells into a self-destructive process. This mechanism was analogous to embedding a self-destructive program within an invasive species, in this case cancer cells, thereby undermining their population stability. The present study, therefore, transitioned from a purely molecular focus to a novel paradigm of cancer ecological regulation. Sch A exploited the evolutionary adaptability of cancer cells, specifically YAP activation, and transformed them into ecologically vulnerable cells through the induction of ferroptosis. This ecological perspective underscores the potential of Sch A to modulate the dynamic interactions between cancer cells and the TME in NSCLC, offering novel avenues for predicting cancer progression and developing more effective therapeutic strategies.

Furthermore, cancer stem cells (CSCs) constitute a small subpopulation within tumors characterized by self-renewal, differentiation and tumor-initiating capacity (33). Numerous studies have demonstrated that lung CSCs are closely associated with recurrence, metastasis and therapeutic resistance in NSCLC, making them both major challenges and important targets in current anticancer strategies (33,34). Although the present study focused primarily on A549 and HCC827 cells, Sch A significantly activated the YAP/ACSL4/TfR signaling axis, leading to intracellular Fe^{2+} accumulation and lipid peroxidation, which are hallmarks of ferroptosis. Notably, previous studies have reported a close relationship between the malignant proliferation of lung CSCs and ferroptosis (35,36). Therefore, the upregulation of TfR induced by Sch A may further sensitize lung CSCs to ferroptotic stress, suggesting that CSCs may serve as potential cellular targets of Sch A. In future studies, it should be investigated whether Sch A can effectively suppress the survival and functionality of lung CSCs through ferroptosis induction, thereby providing a novel approach to overcoming therapeutic resistance in NSCLC.

In conclusion, the results obtained in the present study demonstrated that Sch A induced ferroptosis in lung cancer cells through the YAP/ACSL4/TfR signaling pathway, leading to the disruption of iron homeostasis and the generation of oxidative stress (Fig. 7). This novel mechanism highlights the potential of Sch A as a therapeutic agent that promotes ferroptotic cell death, particularly in the treatment of NSCLC.

Acknowledgements

Not applicable.

Funding

The present work was funded by the Science and Technology Planning Project of Shenzen Municipality (grant no. JSGG20220226090203006).

Availability of data and materials

The data generated in the present study may be requested from the corresponding author.

Authors' contributions

WZ, YC and ZZ designed the research. WZ, YC and XW performed the cell line experiments. XF analyzed the data. YH, YM, QZ and MT performed the animal experiments. WZ, YC, XW and ZZ wrote the manuscript and were responsible for making revisions. ZZ secured funding. All authors confirm the authenticity of all the raw data. All authors read and approved the final manuscript.

Ethics approval and consent to participate

The present study was conducted in accordance with the Animal Research: Reporting of *In Vivo* Experiments guidelines and the Guide for the Care and Use of Laboratory Animals (US National Research Council). All animal experiments were approved by the Committee on the Ethics of Animal Experiments of Guangzhou University of Chinese Medicine (approval no. 2024055R).

Patient consent for publication

Not applicable.

Competing interests

The authors declare that they have no competing interests.

References

1. Cao M and Chen W: Epidemiology of lung cancer in China. Thorac Cancer 10: 3-7, 2019.
2. Li C, Lei S, Ding L, Xu Y, Wu X, Wang H, Zhang Z, Gao T, Zhang Y and Li L: Global burden and trends of lung cancer incidence and mortality. Chin Med J (Engl) 136: 1583-1590, 2023.
3. Li D, Shi J, Liang D, Ren M and He Y: Lung cancer risk and exposure to air pollution: A multicenter North China case-control study involving 14604 subjects. BMC Pulm Med 23: 182, 2023.
4. Fang Y, Li Z, Chen H, Zhang T, Yin X, Man J, Yang X and Lu M: Burden of lung cancer along with attributable risk factors in China from 1990 to 2019, and projections until 2030. J Cancer Res Clin Oncol 149: 3209-3218, 2023.
5. Imyanitov EN, Iyevleva AG and Levchenko EV: Molecular testing and targeted therapy for non-small cell lung cancer: Current status and perspectives. Crit Rev Oncol Hematol 157: 103194, 2021.
6. Xiang Y, Liu X, Wang Y, Zheng D, Meng Q, Jiang L, Yang S, Zhang S, Zhang X, Liu Y and Wang B: Mechanisms of resistance to targeted therapy and immunotherapy in non-small cell lung cancer: Promising strategies to overcoming challenges. Front Immunol 15: 1366260, 2024.
7. Lei G, Zhuang and Gan B: Targeting ferroptosis as a vulnerability in cancer. Nat Rev Cancer 22: 381-396, 2022.
8. Fang K, Du S, Shen D, Xiong Z, Jiang K, Liang D, Wang J, Xu H, Hu L, Zhai X, *et al*: SUFU suppresses ferroptosis sensitivity in breast cancer cells via Hippo/YAP pathway. iScience 25: 104618, 2022.
9. Niu X, Han P, Liu J, Chen Z, Ma X, Zhang T, Li B and Ma X: Regulation of Hippo/YAP signaling pathway ameliorates cochlear hair cell injury by regulating ferroptosis. Tissue Cell 82: 102051, 2023.
10. Cui J, Wang Y, Tian X, Miao Y, Ma L, Zhang C, Xu X, Wang J, Fang W and Zhang X: LPCAT3 is transcriptionally regulated by YAP/ZEB/EP300 and collaborates with ACSL4 and YAP to determine ferroptosis sensitivity. Antioxid Redox Signal 39: 491-511, 2023.
11. Li L, Ye Z, Xia Y, Li B, Chen L, Yan X, Yuan T, Song B, Yu W, Rao T, *et al*: YAP/ACSL4 pathway-mediated ferroptosis promotes renal fibrosis in the presence of kidney stones. Biomedicines 11: 2692, 2023.
12. Wu Z, Sun J, Liao Z, Sun T, Huang L, Qiao J, Ling C, Chen C, Zhang B and Wang H: Activation of PAR1 contributes to ferroptosis of Schwann cells and inhibits regeneration of myelin sheath after sciatic nerve crush injury in rats via Hippo-YAP/ACSL4 pathway. Exp Neurol 384: 115053, 2025.
13. Gu Y, Wu S, Fan J, Meng Z, Gao G, Liu T, Wang Q, Xia H, Wang X and Wu K: CYLD regulates cell ferroptosis through Hippo/YAP signaling in prostate cancer progression. Cell Death Dis 15: 79, 2024.
14. Xiao Z, Xiao W and Li G: Research progress on the pharmacological action of Schisantherin A. Evid Based Complement Alternat Med 2022: 6420865, 2022.
15. Mi X, Zhang Z, Cheng J, Xu Z, Zhu K and Ren Y: Cardioprotective effects of Schisantherin A against isoproterenol-induced acute myocardial infarction through amelioration of oxidative stress and inflammation via modulation of PI3K-AKT/Nrf2/ARE and TLR4/MAPK/NF-κB pathways in rats. BMC Complement Med Ther 23: 277, 2023.
16. Livak KJ and Schmittgen TD: Analysis of relative gene expression data using real-time quantitative PCR and the 2(-Delta Delta C(T)) method. Methods 25: 402-408, 2001
17. Shen Y, Yang Y, Zhao Y, Nuerlan S, Zhan Y and Liu C: YY1/circCTNNB1/miR-186-5p/YY1 positive loop aggravates lung cancer progression through the Wnt pathway. Epigenetics 19: 2369006, 2024.
18. Xie C, Zhou X, Wu J, Chen W, Ren D, Zhong C, Meng Z, Shi Y and Zhu J: ZNF652 exerts a tumor suppressor role in lung cancer by transcriptionally downregulating cyclin D3. Cell Death Dis 15: 792, 2024.
19. Lussier G, Evans AJ, Houston I, Wilsnack A, Russo CM, Vietor R and Bedocs P: Compact arterial monitoring device use in resuscitative endovascular balloon occlusion of the aorta (REBOA): A simple validation study in swine. Cureus 16: e70789, 2024.
20. Jonna S and Subramaniam DS: Molecular diagnostics and targeted therapies in non-small cell lung cancer (NSCLC): An update. Discov Med 27: 167-170, 2019.
21. Wang M, Herbst RS and Boshoff C: Toward personalized treatment approaches for non-small-cell lung cancer. Nat Med 27: 1345-1356, 2021.
22. Feng F, Pan L, Wu J, Liu M, He L, Yang L and Zhou W: Schisantherin A inhibits cell proliferation by regulating glucose metabolism pathway in hepatocellular carcinoma. Front Pharmacol 13: 1019486, 2022.
23. Wang Z, Yu K, Hu Y, Su F, Gao Z, Hu T, Yang Y, Cao X and Qian F: Schisantherin A induces cell apoptosis through ROS/JNK signaling pathway in human gastric cancer cells. Biochem Pharmacol 173: 113673, 2020.
24. Jiang X, Stockwell BR and Conrad M: Ferroptosis: Mechanisms, biology and role in disease. Nat Rev Mol Cell Biol 22: 266-282, 2021.
25. Xian H, Feng W and Zhang J: Schizandrin A enhances the efficacy of gefitinib by suppressing IKKβ/NF-κB signaling in non-small cell lung cancer. Eur J Pharmacol 855: 10-19, 2019.
26. Zhu L, Wang Y, Huang X, Liu X, Ye B, He Y, Yu H, Lv W, Wang L and Hu J: Schizandrin A induces non-small cell lung cancer apoptosis by suppressing the epidermal growth factor receptor activation. Cancer Med 13: e6942, 2024.
27. Nilsson MB, Yang Y, Heeke S, Patel SA, Poteete A, Udagawa H, Elamin YY, Moran CA, Kashima Y, Arumugam T, *et al*: CD70 is a therapeutic target upregulated in EMT-associated EGFR tyrosine kinase inhibitor resistance. Cancer Cell 41: 340-355, 2023.
28. Shyam Sunder S, Sharma UC and Pokharel S: Adverse effects of tyrosine kinase inhibitors in cancer therapy: Pathophysiology, mechanisms and clinical management. Signal Transduct Target Ther 8: 262, 2023.
29. Qian LH, Wen KL, Guo Y, Liao YN, Li MY, Li ZQ, Li SX and Nie HZ: Nutrient deficiency-induced downregulation of SNX1 inhibits ferroptosis through PPARs-ACSL1/4 axis in colorectal cancer. Apoptosis 30: 1391-1409, 2025.
30. Wu X, Sheng H, Zhao L, Jiang M, Lou H, Miao Y, Cheng N, Zhang W, Ding D and Li W: Co-loaded lapatinib/PAB by ferritin nanoparticles eliminated ECM-detached cluster cells via modulating EGFR in triple-negative breast cancer. Cell Death Dis 13: 557, 2022.
31. Luo W: Nasopharyngeal carcinoma ecology theory: Cancer as multidimensional spatiotemporal 'unity of ecology and evolution' pathological ecosystem. Theranostics 13: 1607-1631, 2023.
32. Hsu PC, Yang CT, Jablons DM and You L: The crosstalk between Src and Hippo/YAP signaling pathways in non-small cell lung cancer (NSCLC). Cancers (Basel) 12: 1361, 2020.
33. Liu M, Wu H and Xu C: Targeting cancer stem cell pathways for lung cancer therapy. Curr Opin Oncol 35: 78-85, 2023.
34. Zakaria N, Satar NA, Abu Halim NH, Ngalim SH, Yusoff NM, Lin J and Yahaya BH: Targeting lung cancer stem cells: Research and clinical impacts. Front Oncol 7: 80, 2017.
35. Zheng Y, Yang W, Wu W, Jin F, Lu D, Gao J and Wang S: Diagnostic and predictive significance of the ferroptosis-related gene TXNIP in lung adenocarcinoma stem cells based on multi-omics. Transl Oncol 45: 101926, 2024.
36. Zhou J, Zhang L, Yan J, Hou A, Sui W and Sun M: Curcumin induces ferroptosis in A549 CD133$^+$ cells through the GSH-GPX4 and FSP1-CoQ10-NAPH Pathways. Discov Med 35: 251-263, 2023.